MODELING AND ANALYSIS OF A SINGLE MASS RESONANT GYROSCOPE

S. Sayed[1], A. Badawy[2], S. Wagdy[1] and M. Hegazy[1]

ABSTRACT

Mathematical and simulation models for a single mass resonant gyroscope are discussed in this paper. The mathematical model discusses the dynamics of a single mass that oscillates in two orthogonal directions and subjected to an angular rotation rate about the third direction. The equations of motion are then solved to get the amplitude of the drive and sense mode responses. The solution is applied to a resonant gyroscope. The sense mode response of the gyroscope as subjected to an angular rate input is determined. Sensitivity analysis is then performed to show the effect of the driving force frequency and the natural frequencies of the drive and sense modes. Finite element simulations of a symmetrical resonant gyroscope are presented, and consequently the mechanical coupling between the two vibrating modes is determined. The sense mode response relative to the angular rate input is simulated and the results are compared to the analytical results.

KEY WORDS

Mathematical model, sense mode response, and resonant gyroscope.

[1]   Egyptian Armed Forces.
[2]   Associate Prof., October University for Modern Sciences and Arts- MSA, Egypt.

INTRODUCTION

Micro electromechanical systems (MEMS) are widely used in many fields especially for low cost and low performance applications. Resonant vibratory gyroscopes are one of MEMS sensors that have received a great interest recently. They have met the required specifications of a lot of important applications such as navigation systems, remote devices, automotive industry, and stabilization systems.

However there are recent applications that need the use of high performance MEMS sensors. Increasing the sensitivity and performance of the vibratory gyroscopes has a great deal of research [1-4]. Many key factors can be improved to increase the performance of MEMS sensors such as the fabrication technologies which take a large area of the research development [5, 6]. The sensitivity can be analyzed and optimized during the design process by studying the dynamics of the vibrating structure and modeling the designed device to predict the performance characteristics before the fabrication process. The dynamics are studied and the errors are analyzed in [7, 8]. Finite element simulation is an effective tool for analyzing the operation and the performance of the designed resonant gyroscopes. Simulation models are introduced in [4, 9].

Micro gyroscopes have advantages of miniaturization, low cost and the ability of integrated electronics on the same chip, while the conventional gyroscopes are large and expensive.

Resonant gyroscopes have various vibrating structural elements such as tuning forks, beams, rings and shells. The principle of operation depends on transferring the energy between two vibrating modes due to the Coriolis forces. During operation, a proof mass is driven into vibration by an alternating force (drive mode). When the gyroscope structure is subjected to an angular rotation, secondary oscillations are generated (sense mode) by the Coriolis force. The angular velocity can be determined by measuring the amplitude of the secondary oscillations which are orthogonal to the drive mode.

Symmetrical resonant gyroscope structure has an advantage that the drive and sense natural frequencies are matched. The sensitivity increases when the two natural frequencies are close to each other. It also increases when the drive mode is excited at the resonant frequency that leads to increase the drive mode amplitude and decrease the power needed to drive the proof mass. The drive and sense modes should be mechanically decoupled to achieve stable operation and decrease the gyroscope output at zero rate input.

In section 2, the mathematical model of a single mass resonant gyroscope subjected to an angular rotation is derived showing the response of the drive and sense modes. The effect of matching the resonant frequencies of the two modes is discussed as well as the effect of exciting the drive mode at its natural frequency. Section 3 presents finite element simulations that performed to show the mechanical coupling between the drive and sense modes. The sense mode response relative to the applied angular rate is simulated and the results are compared to the analytical results. Section 4 concludes the results and discusses the future work.

MATHEMATICAL MODEL OF THE RESONANT GYROSCOPE

One of the important factors to improve the performance is introduced by the successful design of the sensors; it will not come without studying the dynamics, analyzing their errors and optimizing parameters to get the required performance characteristics.

For this purpose a mathematical model of the vibrating gyroscope without decoupling frame is derived based on the models presented in [7, 10]. It studies the dynamics of a single mass resonant gyroscope with translation motion of the drive and sense modes and analyzes some design parameters showing their influence on the performance.
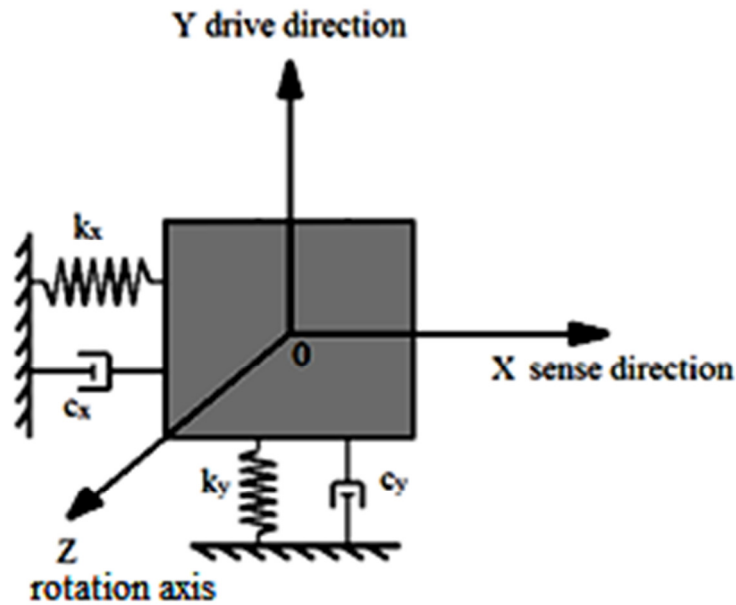

Fig. 1 Schematic diagram of single-mass vibrating gyroscope

Figure 1 shows a schematic diagram of the sensitive element which consists of a proof mass (m) and two equivalent spring systems supporting the proof mass with the base, the primary oscillation direction due to excitation is along Y-axis. When the gyroscope rotates, the secondary oscillation will appear along X-axis due to the Coriolis forces effect.

Let us define orthogonal reference system OXYZ with the origin coincided with the mass center of the proof mass, axis Y is the primary (drive) direction, axis X is the secondary (sense) direction and axis Z is orthogonal to the plane of vibration and represents the rotation axis. The generalized coordinates x, y are the displacements of the proof mass along X axis and Y axis respectively.

The gyroscope is subjected to arbitrary angular velocity Ω that is defined by its components along the defined reference frame as $\mathbf{\Omega} = [\Omega_x \quad \Omega_y \quad \Omega_z]^T$. Position vector of the mass center of the proof mass is $\mathbf{r} = [x \quad y \quad 0]^T$. Then the absolute velocity of the proof mass with respect to the reference frame is:

$$v = [\dot{x} - \Omega_z y \quad \dot{y} + \Omega_z x \quad \Omega_x y - \Omega_y x]^T \tag{1}$$

The kinetic energy and the potential energy of the sensitive element will be:

$$T = \frac{1}{2}m\left((\dot{x} - \Omega_z y)^2 + (\dot{y} + \Omega_z x)^2 + (\Omega_x y - \Omega_y x)^2\right) \tag{2}$$

$$V = \frac{1}{2}k_x x^2 + \frac{1}{2}k_y y^2 \tag{3}$$

where k_x, k_y are the total stiffness of the suspension system in the directions x, y respectively. Using Lagrange equation to determine the equations of motion of two DOF vibrating system

$$\frac{d}{dt}\left(\frac{\partial L}{\partial \dot{q}_i}\right) - \frac{\partial L}{\partial q_i} = Q_i \tag{4}$$

where $(q_i=x, y)$, $L=T-V$, Q_i are the generalized forces, substituting the expressions of the kinetic energy and potential energy in eq. (4), after simplification we can get two ordinary differential equations as

$$\ddot{x} + \left(\omega_{nx}^2 - \Omega_y^2 - \Omega_z^2\right)x - 2\Omega_z \dot{y} + \left(\Omega_x \Omega_y - \dot{\Omega}_z\right)y = q_x \tag{5.a}$$

$$\ddot{y} + \left(\omega_{ny}^2 - \Omega_x^2 - \Omega_z^2\right)y + 2\Omega_z \dot{x} + \left(\Omega_x \Omega_y + \dot{\Omega}_z\right)x = q_y \tag{5.b}$$

where ω_{nx}, ω_{ny} are the natural frequencies in the secondary and primary directions, q_x, q_y are the generalized forces per unit mass in the secondary and primary directions respectively.

These equations represent a system of two differential equations that describes the motion of the proof mass of a single mass resonant gyroscope, by adding damping forces to the system we get

$$\ddot{x} + 2\zeta_x \omega_{nx} \dot{x} + \left(\omega_{nx}^2 - \Omega_y^2 - \Omega_z^2\right)x - 2\Omega_z \dot{y} + \left(\Omega_x \Omega_y - \dot{\Omega}_z\right)y = q_x \tag{6.a}$$

$$\ddot{y} + 2\zeta_y \omega_{ny} \dot{y} + \left(\omega_{ny}^2 - \Omega_x^2 - \Omega_z^2\right)y + 2\Omega_z \dot{x} + \left(\Omega_x \Omega_y + \dot{\Omega}_z\right)x = q_y \tag{6.b}$$

where ζ_x, ζ_y are the damping ratios in the secondary and primary directions.

To determine the angular rate the system of two simultaneous differential equations is solved to get the relation between the displacement and the angular rate. Measuring the displacement of the proof mass in sense direction, the corresponding angular velocity is then determined. In order to simplify the solution the angular velocity is assumed to have one component in the direction perpendicular to the plane of the primary and secondary motions $\Omega = [0 \quad 0 \quad \Omega_z]^T$, and then eqs. (6) is then expressed as:

$$\ddot{x} + 2\zeta_x \omega_{nx} \dot{x} + \left(\omega_{n_x}^2 - \Omega^2\right)x - 2\Omega\dot{y} - \dot{\Omega}y = q_x \tag{7.a}$$

$$\ddot{y} + 2\zeta_y \omega_{ny} \dot{y} + \left(\omega_{ny}^2 - \Omega^2\right)y + 2\Omega\dot{x} + \dot{\Omega}x = q_y \tag{7.b}$$

Here, a set of parameters can describe the dynamics of the vibrating gyroscope motion as follows: ω_{nx}, ω_{ny} are the natural frequencies in the secondary and primary directions, ζ_x, ζ_y are the damping ratios, ω is the frequency of the excitation force. These parameters can control the sensitivity, resolution, operating range and bias of the resonant gyroscopes, so adequate design of them is needed to achieve the required performance of the gyroscope. Given constant angular velocity, Eqn. (7) renders to:

$$\ddot{x} + 2\zeta_x \omega_{nx} \dot{x} + \left(\omega_{nx}^2 - \Omega^2\right)x - 2\Omega\dot{y} = q_x \tag{8.a}$$

$$\ddot{y} + 2\zeta_y \omega_{ny} \dot{y} + \left(\omega_{ny}^2 - \Omega^2\right)y + 2\Omega\dot{x} = q_y \tag{8.b}$$

The system of differential equations is then solved in order to study the motion of the proof mass of the vibrating gyroscope subjected to constant angular velocity along Z-axis and no external forces acting along the sense direction $q_x(t)=0$. In the case of completely decoupled modes, the displacement in the secondary direction will depend only on the angular velocity.

Let the excitation force be harmonic and it can be represented in a complex form as $q_y(t) = q_y e^{i\omega t}$ where q_y is the amplitude of the excitation force and ω is the frequency of the excitation force. Since the excitation is harmonic and it is given only by the real part of $q_y(t)$, the response of the primary and secondary oscillations will also be given only by the real part of $y(t)$ and $x(t)$ respectively [11]. Then, the particular solution is represented in a complex form as:

$$x(t) = Xe^{i\omega t} \tag{9.a}$$

$$y(t) = Ye^{i\omega t} \tag{9.b}$$

and

$$X = X_0 e^{i\phi_x} \tag{10.a}$$

$$Y = Y_0 e^{i\phi_y} \tag{10.b}$$

where X_0, Y_0 are the amplitudes of the secondary and primary vibrations respectively and ϕ_x, ϕ_y are their phases. After solving the system of differential equations, the amplitudes of the secondary and primary vibrations are expressed as:

$$X_0 = \frac{2q_y \omega\Omega}{\Delta_0} \tag{11}$$

$$Y_0 = \frac{q_y \sqrt{\left(\omega_{nx}^2 - \Omega^2 - \omega^2\right)^2 + \left(2\zeta_x \omega_{nx} \omega\right)^2}}{\Delta_0} \tag{12}$$

where

$$\Delta_0^2 = \left[\left(\omega_{nx}^2 - \Omega^2 - \omega^2\right)\left(\omega_{ny}^2 - \Omega^2 - \omega^2\right) - 4\omega^2\left(\zeta_x \omega_{nx} \zeta_y \omega_{ny} + \Omega^2\right)\right]^2$$
$$+ 4\omega^2 \left[\zeta_x \omega_{nx}\left(\omega_{ny}^2 - \Omega^2 - \omega^2\right) + \zeta_y \omega_{ny}\left(\omega_{nx}^2 - \Omega^2 - \omega^2\right)\right]^2$$

The relation between the angular rate and the amplitudes of the primary and secondary vibrations are then obtained. Once the secondary amplitude of the resonant gyroscope is measured, the corresponding angular rate can be determined. The driving force frequency is an important parameter in the design of the resonant gyroscope. To show the effect of changing the driving force frequency on the sense mode amplitude, a dimensionless parameter (r) is introduced where (r= ω/ω_{ny}) is the ratio of the driving force frequency and the primary mode natural frequency.

Figure 2 shows the relation between the sense mode amplitude and the angular rate applied to the gyroscope at different values of r. One can see that the deviation of the driving frequency from the primary natural frequency leads to a decrease in the sensitivity and in the resolution of the resonant gyroscope. But it has an advantage that it increases the measurement range of the external angular rate.

A trade-off between the sensitivity and the measurement range of the gyroscope is then needed in considering the design process to cover the operating range required with a suitable sensitivity. It is assumed that the natural frequency values are similar during this analysis.
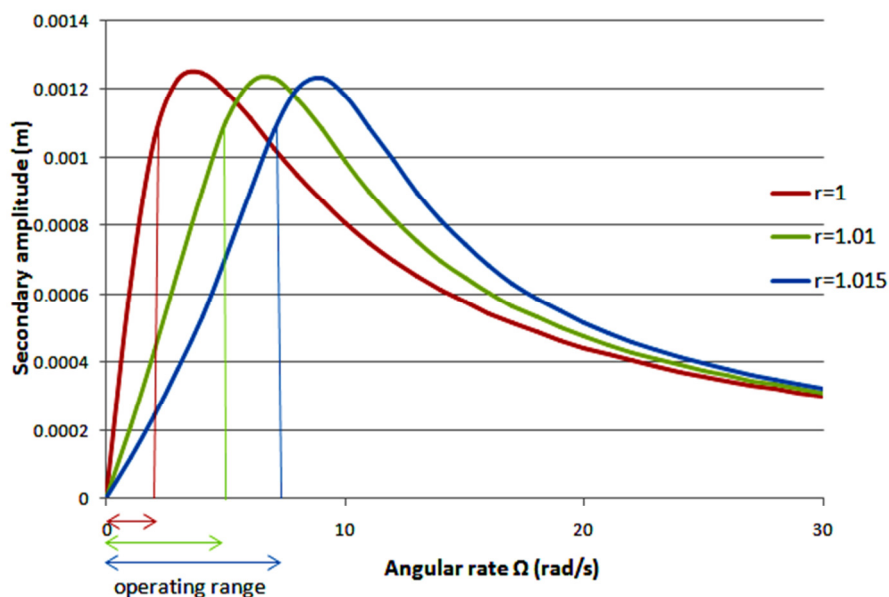

Fig. 2 Secondary amplitude response with the angular rate at different values of frequency ratio (r)

Figure 3 describes the behavior of the sensitive element when the two resonant frequencies are matched or separated. The figure shows that the sensitivity reaches its maximum value when the primary and secondary natural frequencies are matched (i.e. $\omega_{nx}=\omega_{ny}$) which is an advantage of using a symmetric design of the resonant gyroscope. When the two frequencies have different values the sensitivity decreases significantly.

Although the sensitivity is maximum at $\omega_{nx}=\omega_{ny}$, the bandwidth is minimum. The secondary oscillations amplitude is sensitive to the changes in the bandwidth, for a wide bandwidth range, the secondary vibration amplitudes are nearly constant. This is a trade-off between using matched frequencies for increasing sensitivity and using separated frequencies for increasing bandwidth, so the ratio between the resonant frequencies should be designed giving the necessary bandwidth.
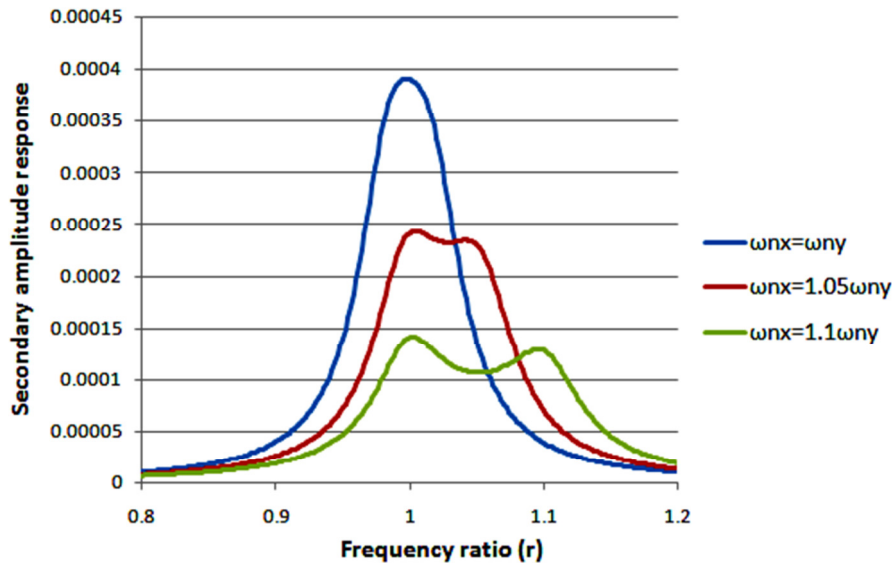
Fig. 3 Secondary amplitude response with the frequency ratio showing the effect of natural frequencies separation on the sensitivity and bandwidth

The mathematical model is applied to the resonant gyroscope presented in [12] to get the secondary motion amplitude response relative to the angular rate input. Using the resonant gyroscope model data for the primary and secondary resonant frequencies, the frequency ratio equals 0.98 (i.e. r=0.98).

Figure 4 shows the amplitude of the secondary motion with the angular velocity applied to the resonant gyroscope. The response is approximately linear in a limited range which is the linear measurement range of the gyroscope. Therefore the operating angular rate range will be from 0 to 9 rad/sec.
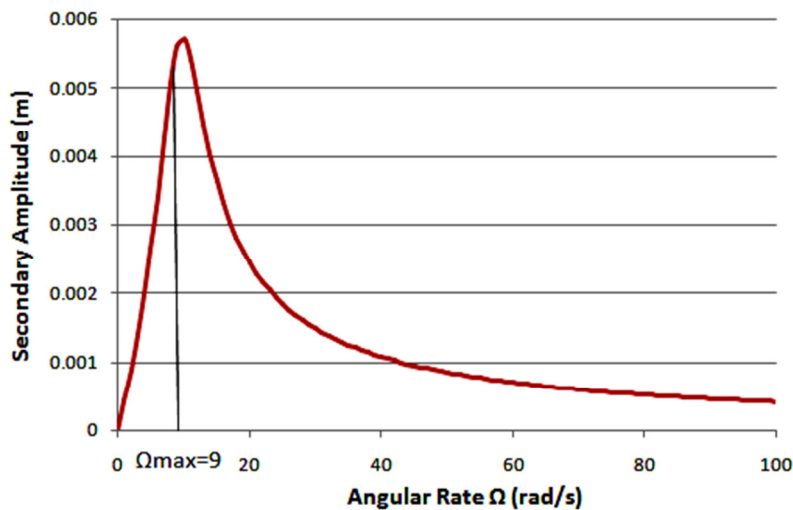

Fig. 4 Secondary vibrations amplitude of the designed resonant gyroscope

FINITE ELEMENT MODEL

Finite element simulations are performed using ANSYS software. The simulated results are used to verify the results determined from the mathematical model. The finite element simulations are applied to the gyroscope model presented in [12], in

which the boundary conditions at the ends of the beams are fixed. The element type used in the finite element model is solid 186 with tetrahedral shape. The material used for the model is aluminum alloy 2024.

The drive and sense modes are assumed to be completely decoupled in the mathematical model and they are coupled only by the angular rotation rate. Finite element simulation shows that the amount of mechanical coupling between the two vibrating modes is low.

Figure 5 shows the finite element simulation of the relative displacement for the two vibration modes when only one mode is under vibration. It shows that during the vibration of one mode, the second mode is slightly affected by the vibration of the first mode. From this simulation, the mechanical coupling between the drive and sense mode is less than 4% of the vibration amplitude.
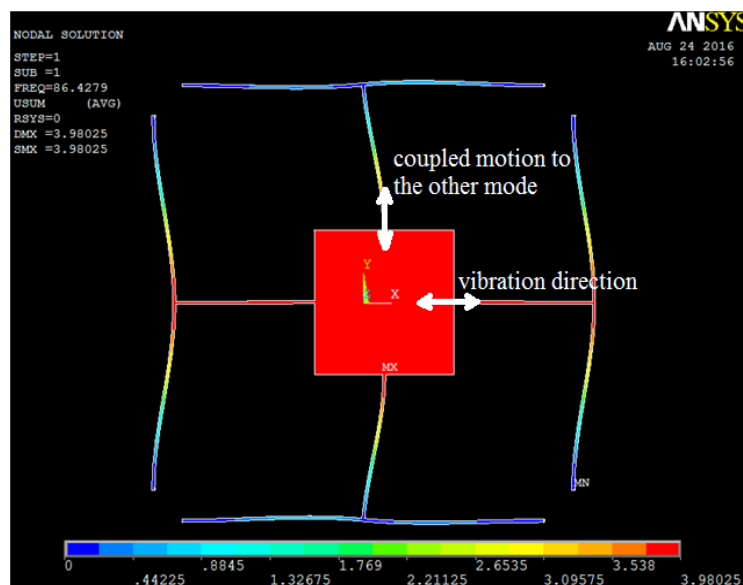

Fig. 5 ANSYS finite element simulation of the relative displacement for the two vibration modes when only one mode is vibrating, the mechanical coupling between them is less than 4%

The overall operation of the resonant gyroscope is simulated to show the response of the secondary motion of the gyroscope when it is applied to angular rate input in the existence of the driving force excitation. Figure 6 shows the motion of the sense mode coupled with the drive mode due to the effect of the Coriolis force induced from the angular rate input to the gyroscope.

The results determined from the simulations are compared to the analytical results to verify the sense mode amplitude response of the resonant gyroscope. Figure 7 shows the analytically calculated secondary amplitude compared with the simulated amplitude. As shown in the figure, the simulated secondary amplitude response is closely matched the calculated results in the operating measurement range (Ωmax) which satisfies the theoretical analysis. The difference between the two results at higher angular rates comes from the increasing of the mechanical coupling between the drive and sense modes at higher angular rates which are assumed to be completely decoupled in the theoretical analysis and the two modes are only coupled by the effect of the Coriolis forces.
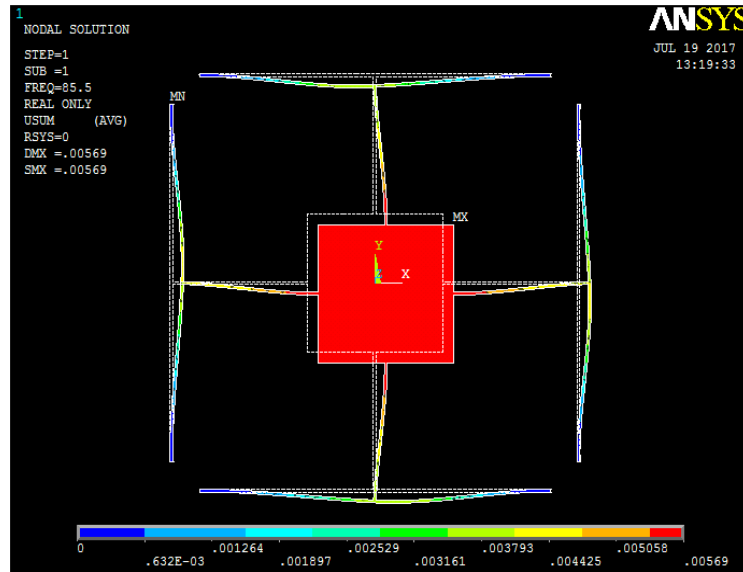
Fig. 6 The secondary motion under the effect of the Coriolis force due to an applied angular rate
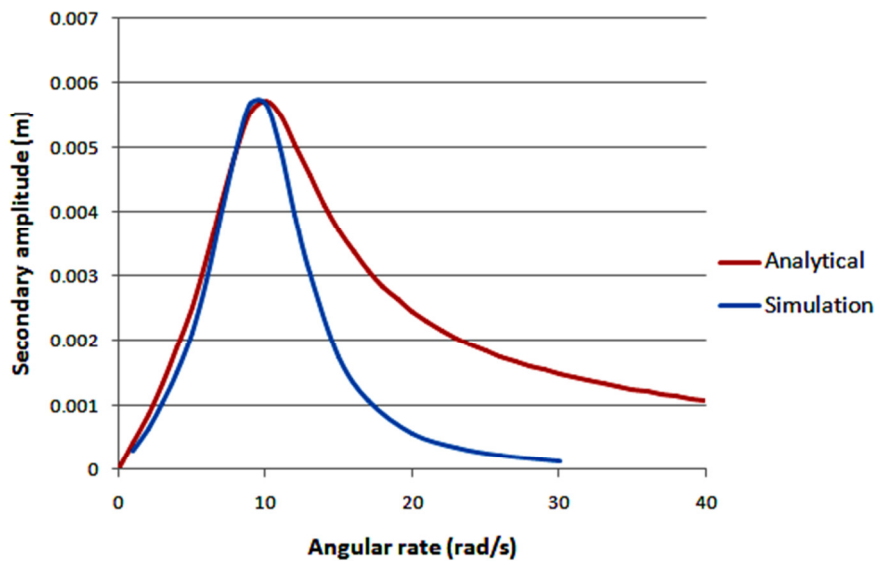

Fig. 7 Simulated secondary amplitude of the resonant gyroscope compared with the analytically calculated results

CONCLUSIONS

The drive and sense mode responses of a single mass resonant gyroscope are determined by studying the dynamics of the system and solving the equations of motion. The drive and sense modes are coupled only by the applied angular rate. The amplitude of the sense mode response depends on the Coriolis forces generated due to the angular rate input. The analysis shows that the sensitivity increases when the driving force frequency equals the resonant frequency of the drive mode. On the other hand, the measurement range increases when the frequencies of the driving force and the drive mode are different. The sensitivity also

increases when the natural frequencies of the drive and sense modes are matched which is an advantage of the symmetrical gyroscope structure. Finite element simulations of the designed resonant gyroscope are presented. The mechanical coupling between the drive and sense modes is 4%. The response of the resonant gyroscope is simulated when it is subjected to angular rotation input. The amplitude of the sense mode response is determined. The results are close to the analytical results in the operating range. The simulated results verify the theoretical analysis.

REFERENCES

[1]   F.-Y. Lee, K.-C. Liang, E. Cheng, S.-S. Li, and W. Fang, "Acceleration-insensitive fully-decoupled tuning fork (FDTF) MEMS vibratory gyroscope with 1/HR BIAS instability," in Micro Electro Mechanical Systems (MEMS), 2016 IEEE 29th International Conference on, 2016, pp. 946-949.

[2]   J. Zhou, T. Jiang, J.-w. Jiao, and M. Wu, "Design and fabrication of a micromachined gyroscope with high shock resistance," Microsystem Technologies, vol. 20, pp. 137-144, 2014.

[3]   M. F. Zaman, A. Sharma, Z. Hao, and F. Ayazi, "A mode-matched silicon-yaw tuning-fork gyroscope with subdegree-per-hour Allan deviation bias instability," Journal of Microelectromechanical Systems, vol. 17, pp. 1526-1536, 2008.

[4]   S. E. Alper, K. Azgin, and T. Akin, "A high-performance silicon-on-insulator MEMS gyroscope operating at atmospheric pressure," Sensors and Actuators A: Physical, vol. 135, pp. 34-42, 2007.

[5]   S. E. Alper and T. Akin, "A single-crystal silicon symmetrical and decoupled MEMS gyroscope on an insulating substrate," Journal of Microelectromechanical Systems, vol. 14, pp. 707-717, 2005.

[6]   J.-T. Liewald, B. Kuhlmann, T. Balslink, M. Trächtler, M. Dienger, and Y. Manoli, "100 kHz MEMS vibratory gyroscope," Journal of Microelectromechanical Systems, vol. 22, pp. 1115-1125, 2013.

[7]   V. Apostolyuk and F. E. Tay, "Dynamics of micromechanical coriolis vibratory gyroscopes," Sensor Letters, vol. 2, pp. 252-259, 2004.

[8]   S. W. Yoon, S. Lee, and K. Najafi, "Vibration-induced errors in MEMS tuning fork gyroscopes," Sensors and Actuators A: Physical, vol. 180, pp. 32-44, 2012.

[9]   Y. Guan, S. Gao, H. Liu, and S. Niu, "Acceleration sensitivity of tuning fork gyroscopes: Theoretical model, simulation and experimental verification," Microsystem Technologies, vol. 21, pp. 1313-1323, 2015.

[10]   V. A. Apostolyuk, V. Logeeswaran, and F. E. Tay, "Efficient design of micromechanical gyroscopes," Journal of Micromechanics and Microengineering, vol. 12, p. 948, 2002.

[11]   S. S. Rao and F. F. Yap, Mechanical vibrations vol. 4: Prentice Hall Upper Saddle River, 2011.

[12]   S. Sayed, S. Wagdy, A. Badawy, and M. Hegaze, "Symmetrical In-Plane Resonant Gyroscope with Decoupled Modes," World Academy of Science, Engineering and Technology, International Journal of Mechanical, Aerospace, Industrial, Mechatronic and Manufacturing Engineering, vol. 11, pp. 255-260, 2017.